Numerical Study of Geogrid-Reinforced Retaining Wall

Marwa Feligha[1], Fatima Zohra Benamara[2], Nouaouria Mohamed Salah[2], Benayoun Fadila[3], and Souhila Rehab Bekkouche[1]
[1]*University 20 Augest1955, Skikda, Faculty of Technology, Department of Civil Engineering, LMGHU Laboratory, Algeria*
[2]*University 8 May 1945, Faculty of Sciences and Technology, Laboratory of Civil Engineering and Hydraulics (LGCH), Algeria*
[3]*University of Larbi Ben M'hidi, Oum El Bouaghi, Faculty of Sciences and Applied Sciences, Department of Civil Engineering, LDDPE Laboratory, Algeria*
E-mail: feligha_marwa@yahoo.com

ABSTRACT: The use of geogrid-reinforced soil retaining walls has increased considerably due to several advantages, such as their relative and rapid construction, aesthetics, and good seismic performance. The behavior of these structures is complex, which requires research to better understand the effect of certain parameters on the behavior of geogrid-reinforced soil structures. The aim of this work is the numerical modeling of geogrid reinforced soil retaining wall with a segmental-facing geogrid-reinforced retaining wall using the finite element code (PLAXIS^{2D}). The objective of this work is to investigate the influence of some geometrical and mechanical parameters on the behaviour of a geogrid-reinforced soil retaining wall to analyze numerically the peak tensile strength, lateral facing displacements, critical failure surfaces and safety factor. The numerical results show that the failure plane occurred in the reinforced zone at the mid-height; this observation contradicted the triangular distribution with depth assumed in conception methodologies for reinforced soil retaining wall. The distribution of peak tensile strength with depth was bilinear at high-loading increments and became trapezoidal at low-loading ones.

Furthermore, it was found that the behaviour of a geogrid-reinforced soil retaining wall is independent of loading increments width beyond 0.5H, which coincides with the Ranking failure surface. It also seems that the location of the loading increments and the loading values can change the shape and the position of the peak tensile strength mobilized along the geogrid from a position closer to the facing to the soil reinforcement, which is more pronounced for the higher loading values. As far as the present study is in agreement with the AASHTO conception method, according to which the failure surface was based on the Rankine plane for a vertical facing and the Coulomb plane with an inclined facing $\omega \geq 10°$. It also seems that the geogrid inclination angle has a major effect on the lateral facing displacements and safety factor; these results have major implications for conception. The soil-geogrid friction ratio is not considered to have a major effect on the peak tensile strength value for a friction ratio greater than $4/7\varphi$.

KEYWORDS: Failure surface, PLAXIS^{2D}, Retaining walls, Reinforced soil, and Tensile strength.

1. INTRODUCTION

Geogrid-reinforced soil retaining wall has been developed for a wide variety of applications in several fields (geotechnics, hydraulics, mechanics, engineering, etc.). This latter was a composite structure formed by soil-geogrid interaction. The main function of the geogrid layers was to improve the tensile strength of soil. Reinforced soil retaining wall was calculated using the conception method of the American Association of State Highway and Transportation Officials (AASHTO, 2012), which were based on the limit equilibrium approach. This conception method neglects several parameters that affect the performance of reinforced soil retaining walls.

Ho (1993) performed numerical simulations using the finite element program AFENA to study the influence of several geometrical and mechanical parameters on the behavior of the reinforced retaining wall, postulating that the most important factors affecting the peak tensile strength were: reinforcement stiffness density; facing-soil friction factor; soil friction angle; and facing rigidity.

Bathurst and Hatami (1998) used the two-dimensional, explicit finite difference program (FLAC) to perform the numerical experiments. They indicated that the results of the lateral facing displacement and the peak tensile strength of the reinforcement are in agreement with the results of Rowe and Ho (1997).

To study the effect of loading increments, Haza (1997) performed full-scale tests to validate double block method based on the limit equilibrium approach, which consists of locating the failure surfaces to calculate the peak tensile strength and the safety factor. He showed that this method gives a conservative solution in several cases.

Djebablah et al. (2020) carried out a numerical research of a geosynthetic reinforced soil walls, using the FLAC^{2D} (Fast Lagrangian Analysis of Continua). The numerical results show that peak tensile strength in the reinforcement layers and lateral displacement of the facing increase with increasing uniform loading increments.

The numerical analysis to study the influence of facing inclination angle was examined by Rahmouni et al. (2016). The results show that the peak tensile strength decreases with increasing facing inclination angle. In order to examine the behavior of geosynthetic reinforced soil retaining wall, Yang et al. (2013) used the PLAXIS^{2D} finite element code. The comparison of numerical and experimental results show that predictedpeak tensile strength in the reinforcement layers at the end of construction were closer to the measured values.

The width and position of loading are one factor that changes the response of reinforced retaining walls, have been the subject of experimental and numerical works (Laboudi et al., 2022); Mariano et al. (2021); Djebablah et al. (2020); Mirmoradi and Ehrlich (2019).

The present paper aims to evaluate the influence of loading increments, loading increments width, loading increments location, facing inclination angle, geogrid inclination angle, and geogrid-soil friction factor on the behaviour of a geogrid-reinforced soil retaining wall to analyze peak tensile strength, lateral facing displacements, critical failure surfaces, and safety factor, using the PLAXIS^{2D} code.

2. MODELS FOR MECHANICAL FAILURE

The stability conditions of geogrid-reinforced soil retaining walls are influenced by the geometry, the soil mechanical properties, and the soil-reinforcement interaction mechanism. The principle of failure detection can be summarized in two steps:

- the objective of the first step is to identify the geometrical configurations favorable to failure for the different known failure mechanisms.

- the second step involves the calculation of the safety factors associated with each failure mechanism identified in the previous step.

We assume that the critical failure surface of a reinforced earth wall coincides with the line of peak tensile strength, i.e., the critical failure surface is located according to the points of peak tensile strength in each reinforcement layer (Figure 1).

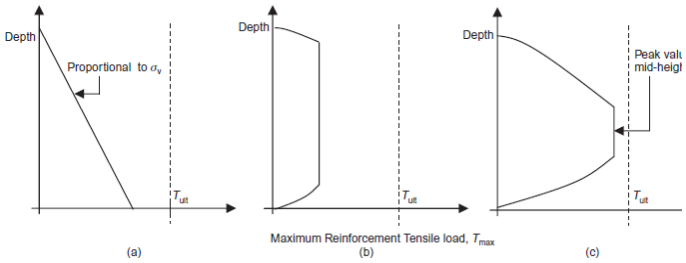

Figure 1 Location of tensile strength reinforced soil retaining walls: (a) design methodologies for geosynthetic walls; (b) uniform distribution for low loading increments; (c) trapezoidal distribution for high loading increments (Yang et al., 2012)

3. NUMERICAL MODEL

3.1 Reference Case Definition

The reference case was 6 m high and 13 m long from the facing (Figure 2), with a segmental facing of thickness 0.14 m. The geogrid layers were placed horizontally with a length of 4.25 m which is around 0.7 H to meet the AASHTO conception method and spaced 1 m apart vertically. Also, the building phasing was respected. The geometry of the model examined in this paper was shown in Figure 2. The plane deformation behavior of this wall was simulated by Bathurst and Hatami (1998) using the FLAC code based on the finite difference method.

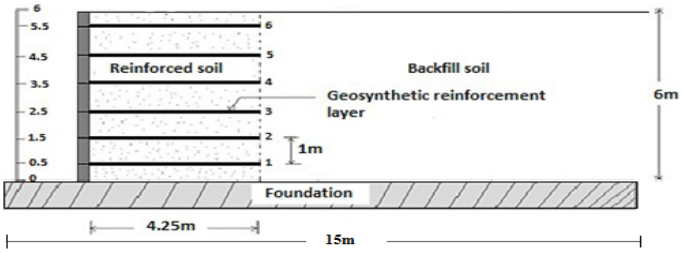

Figure 2 Geometry of numerical reference model (Djebablah et al., 2020)

Figure 3 shows the numerical model used in this investigation. The elastic perfectly plastic model with the Mohr-Coulomb criterion was adopted to model the reinforced and unreinforced soil; moreover, the facing was modeled by three-node beam elements called "plate" in PLAXIS^{2D} code. The foundation was assumed to be rigid and had a unit weight of 23 kN/m^3; its behavior was governed by linear elastic criterion. The soil-geogrid, soil-foundation, and soil-facing contact was modeled by a rigid interface element with an interface friction angle of 20°. The reinforcement layers were simulated using six geogrid elements that are available in PLXIS^{2D}; the axial stiffness was taken as E.A. = 2000 kN/m. This latter was chosen with linear elastic behavior, and the creep phenomenon is neglected. The materials' properties were estimated from the studies performed by Bathurst and Hatami (1998), as summarized in Table 1.

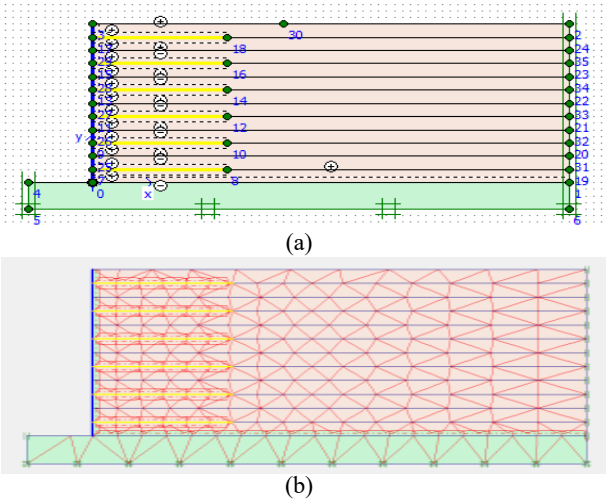

(a)

(b)

Figure 3 Numerical model (a) Cross-sectional view (b) meshes for the reference case.

Table 1 Index properties of soil reinforcement and facing

Soil reinforcement		**Elastic perfectly plastic model (Mohr-Coulomb)**	
	ν	Poisson's ratio	0.3
	ψ	Dilatancy angle (°)	5
	ϕ	Friction angle (°)	35
	c	Cohesion (kPa)	1
	E	Young's modulus (kN/m^2)	35000
	γ	Unit weight (kN/m^3)	20
Facing		**Elastic Plate Element**	
	E.A.	Normal stiffness (kN/m)	5.10^6
	EI	Flexural rigidity (kN.m^2/m)	8.5.10^3

3.2 Validation of the Numerical Model

In the first stage of this study, a series of analyses were performed to validate our model and for the parametric study to be reliable. The numerical model, reported by Rowe and Ho (1997), has been considered by several researchers, such as Djebablah et al. (2020), Vieira et al. (2008), and Bathurst and Hatami (1998). These results were also used to validate the numerical model developed in this study because it presents a good characterization of the materials and a good construction sequence.

Figure 4(a) shows a comparison between the numerical results for peak tensile strength at the end of construction under the effect of the self-weight adopted from this study and the results obtained by Djebablah et al. (2020), Vieira et al. (2008) and Rowe & Ho (1997). It can be seen that the numerical results of the peak tensile strength were in good agreement with those of the above authors.

Figure 4(b) presents lateral facing displacement. It seems to be in accordance with the results obtained by the above-mentioned authors. With the exception of the third upper part of the wall, the lateral displacement decreases. The difference may be due to the treatment with the segmental facing panel. The maximum lateral displacement obtained for this case was about 25.72 mm which presents a strain of about 4.73% located at the interface between the reinforced soil and the facing.

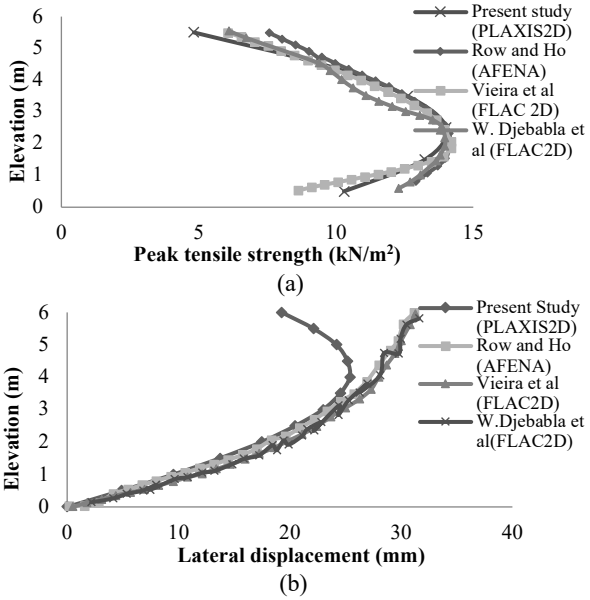

Figure 4 Comparison results (a) peak tensile strength and (b) lateral facing displacement

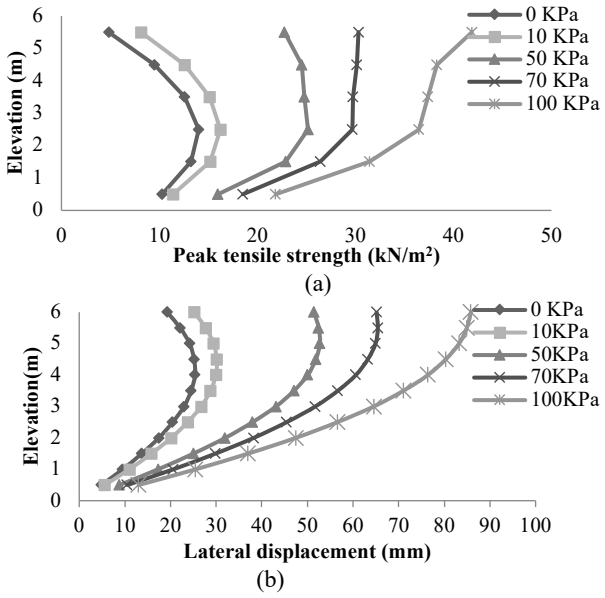

Figure 5 Effect of loading increments: (a) peak tensile strength (b) lateral facing displacement

3.3 Effect of Loading Increments

The effect of loading increments ranging from 0 kPa, 10 kPa, 50 kPa, 70 kPa, and 100 kPa, on the peak tensile strength and the lateral facing displacement is illustrated in Figure 5(a, b).

According to the results obtained, we notice an increase of the peak tensile strength in the geogrid layers with the increase of loading increments. A trapezoidal shape of peak tensile strength with depth at low loading increments (<50kPa), with the critical value, was located at a height of 0.5H above the base of wall. This value seems to agree with the results obtained in the bibliographical research. Yang et al. (2012).

Yang et al. (2012) carried out centrifuge tests in geosynthetic reinforced soil slopes. Also, this model was numerically analyzed by the finite element method to investigate the distribution and development of soil stresses and peak tensile strength. They postulated that the peak value of tensile strength was positioned approximately halfway up the reinforced slopes. Furthermore, Zornberg and Arriaga (2003) carried out scale models with digital image analysis to evaluate the deformation distribution in the geosynthetic reinforced soil. They found that the location of critical deformation of the reinforcement was not at the base of the slope but was approximately located at the mid-height of the slope. The distribution of the peak tensile strength at high loading increments (>50kPa) depicts a bilinear distribution. It was noted that similar results were reported by Woodruff (2003). The distribution of peak tensile strength in the current study does not follow the triangular distribution with depth assumed in geogrid–reinforced retaining wall conception methodologies. It can be observed that the lateral displacement increases with increasing loading increments.

The calculation of the safety factor (Fs) in PLAXIS^{2D} can be done by reduction of strength parameters c and tanϕ until failure is achieved. This process is called "Phi-C reduction" and resembles the safety factor calculation method conventionally adopted in sliding critical failure surfaces. The incremental multiplier (ΣMsf) used to define the value of the soil characteristics at a given stage of the analysis (equation 1):

$$\Sigma M_{sf} = \frac{tan\varphi_{input}}{tan\varphi_{reduced}} = \frac{c_{input}}{c_{reduced}} \quad (1)$$

Figure 6 shows that, as loading increments increase (from 0 kPa to 100 kPa), the magnitude for the safety factor decreases. Also, it can be seen that the geogrid-reinforced soil retaining wall is unstable when loading increments was greater than 90 kPa. The required safety factor for reinforcement stability, recommended by AASHTO (2012), equals to 1.5.

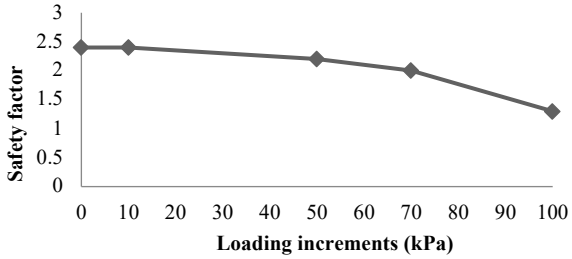

Figure 6 Safety factor for different loading increments

3.4 Effect of Loading Increments Width (l)

The evaluation of reinforced soil retaining wall behavior subjected to five different loading increments widths (l = 1.2m, 2.92m, 4.25m, 6m, and 15m) are summarized in Figure 7.

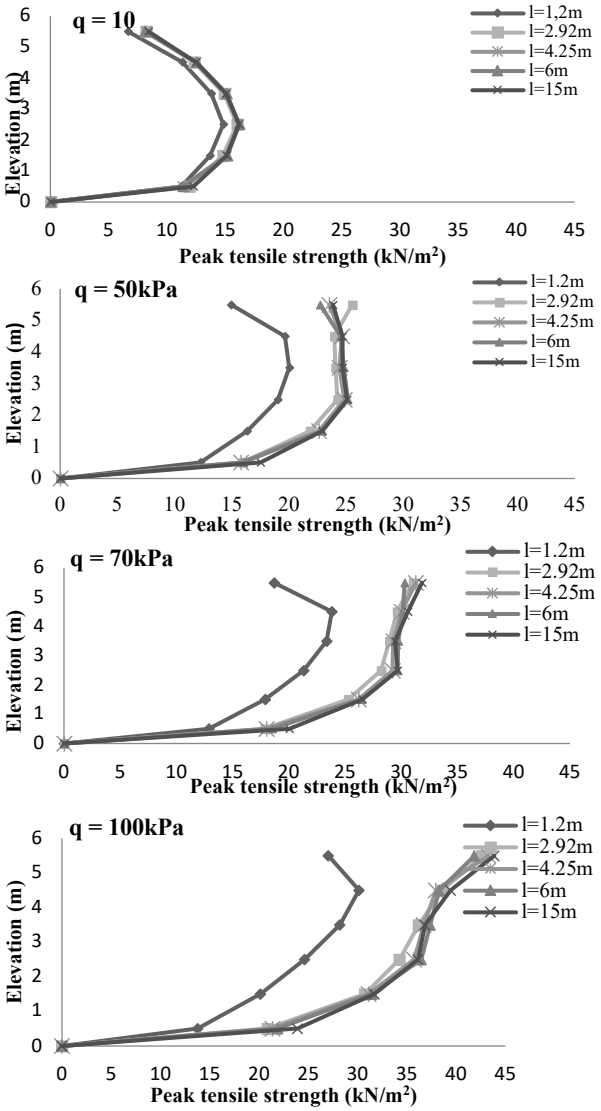

Figure 7 Effect of different loading increments width on peak tensile strength

The peak tensile strength increases with increasing of loading increments width; this increase was less important for the lower layers because of the distribution of loading with depth. The increase of loading increments width beyond 0.5H (l=2.92m) has practically no effect on the distribution of peak tensile strength, which coincides with Rankine's failure surface. Note that the AASHTO (2012) conception method does not take into account the loading increments applied on the unreinforced soil for the calculation of peak tensile strength (maximum width of 0.7H), which leads to an underestimation of the tensile strength of the reinforcement layers. It is noted that similar results reported by Djebablah et al. (2020) show that the width (6m and 8m) of different loading increments applied have no effect on the normalized peak tensile strength. Mariano et al. (2021) carried out a numerical study to evaluate the effect of the loading width on the behavior of the reinforced soil retaining walls. Increasing the width of the loading for small height walls (H = 3.6m) does not affect the distribution of normalized peak tensile strength, while for large height walls (H = 6.2m and H = 12.4m), the normalized peak tensile strength increases with increasing loading width.

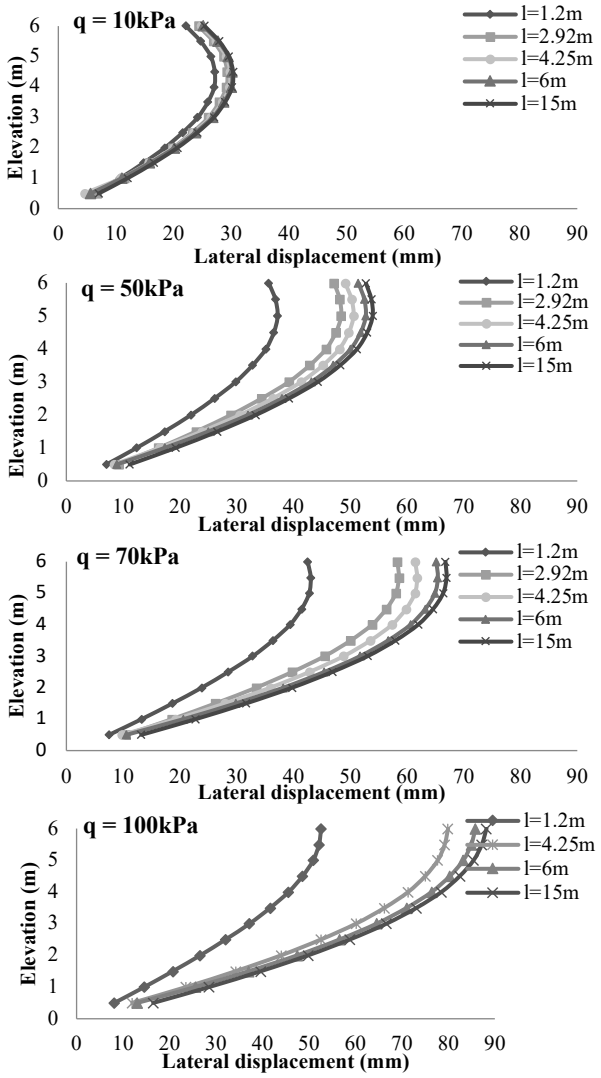

Figure 8 Effect of different loading increments width on lateral facing displacement

In order to assess the effect of different loading increments width on the lateral facing displacement, the results are presented in Figure 8. No trend was observed regarding the values of lateral facing displacement, which appear not to be affected by the loading increments width beyond 0.5H (l = 2.92m), regarding the low value of q = 10kPa. For high loading increments (q≥50 kPa), the lateral facing displacement increases with increasing different loading increments width.

3.5 Effect of Loading Increments Location

A cross-sectional of the position of loading increments location is shown in Figure 9.

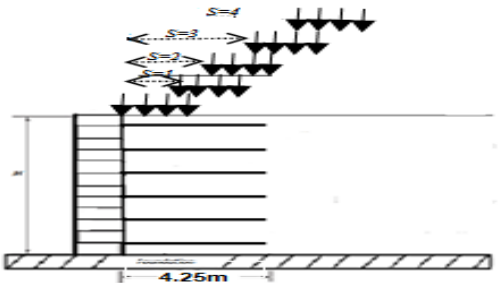

Figure 9 Position of loading increments location

The peak tensile strength measured at the geogrid layers for the same loading increment width (l = 2.92 m) under different loading increments locations (s = 0m; 1m; 2m; 3m; 4m) is illustrated in Figure 10.

The comparison of the curves shows that the increase in loading increments locations decreases the peak tensile strength in the geogrid layers. Furthermore, the loading increments location applied for s = 3m and s = 4m has no effect on the peak tensile strength. The position of the peak tensile strength mobilized along the geogrid layers depends on the loading increments location conditions, where this latter was transferred from geogrid layer 3 to geogrid layer 2. This phenomenon is more pronounced for the higher loading values. This coincides with the results of the experimental study of Mirmoradi and Ehrlich (2019). As observed, the same shape (trapezoidal) was obtained for all loading increment locations for q = 10 kPa, while for q> 50 kPa, the development of the curves shape changed with the loading increments location, exhibiting a bilinear distribution for s = 0m to a trapezoidal distribution for other locations (s =1m, 2m, 3m, and 4m). These results highlight the importance of loading increment location for the failure mechanism.

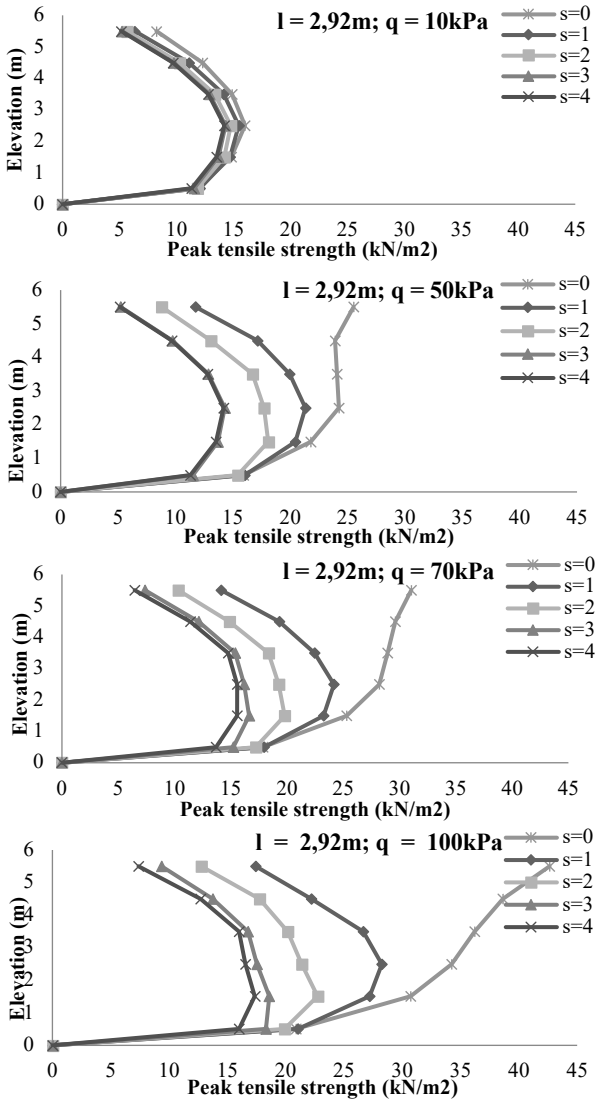

Figure 10 Effect of different loading increment locations on peak tensile strength

In order to evaluate the effect of loading locations on the peak tensile strength, the results are also presented in Figure 11 in the form of column graphs that consist of four categories, each representing a loading location. It shows the peak tensile strength of different loadings increments (10 kPa; 50 kPa; 70 kPa; 100 kPa) with different loading widths (l = 1.2m; 2.92m; 6m). It noted that no trend was observed in the values of the peak tensile strength, which seem to be unaffected by the width and the location of low load (q = 10 kPa). In addition, it should also be noted that the peak tensile strength decreases with increasing loading location of different widths of applied loading for q≥ 50 kPa, except the case where s = 3m and s = 4m found approximately the same values.

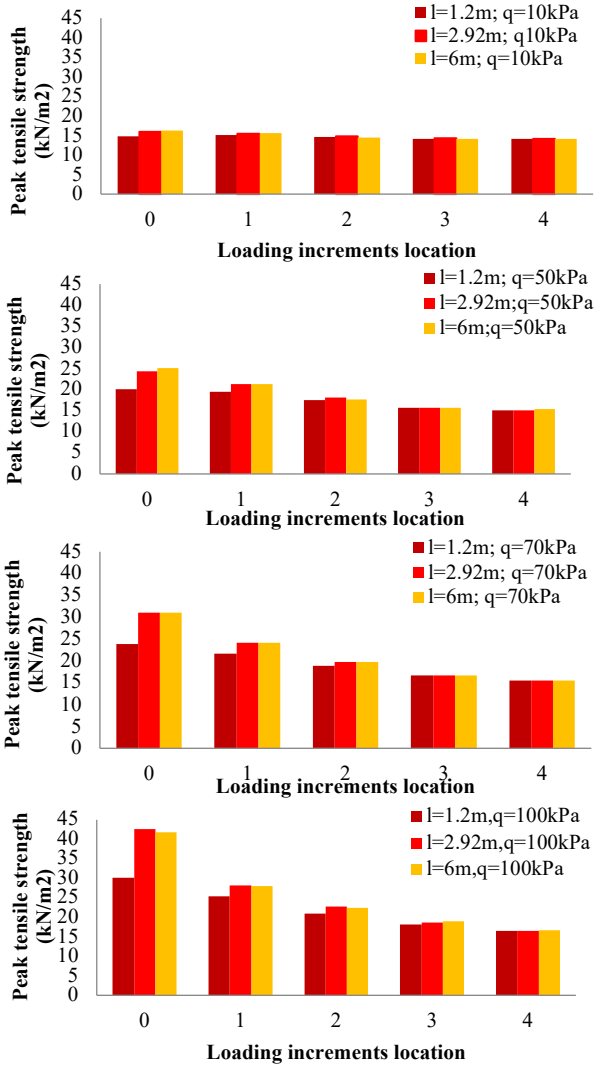

Figure 11 Column charts of loading increment location for different loading width

3.6 Effect of Facing Inclination Angle (ω)

The facing inclination angle (ω) is one factor that changes the response of geogrid-reinforced retaining wall. In order to evaluate the effect of this latter, the analyses were performed considering four values of ω = 5°, 10°, 15°, 20°.

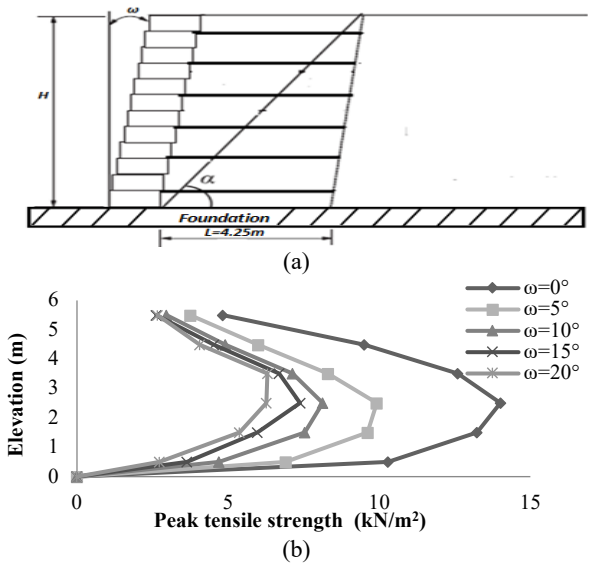

Figure 12 (a) Location of internal failure surface; (b) influence of facing inclination angle on peak tensile strength

Figure 12(b) shows that as the inclination angle decreases, the magnitude of peak tensile strength at each elevation increases also. These results can be justified by the reduction in the earth pressure coefficient k_a, which was computed using Coulomb's theory, that accounts for the effect of the facing inclination angle and soil-facing friction ratio. Also, the shape of the distribution of maximum tensile strength with depth was considered to be trapezoidal rather than linear, as assumed by earth pressure theory according to equation 2 recommended by the AASHTO (2012) design method.

$$k_a\,(\gamma H + q)S_v \tag{2}$$

where: ɣ: unit weight of soil; H: wall height; S_v: vertical spacing of geogrid; q: loading increments.

The earth pressure coefficient was calculated using equation (3) (Rankine theory for vertical facing).

$$k_a = \tan^2\left(\frac{\pi}{4} - \frac{\varphi}{2}\right) \tag{3}$$

For inclined facing, the earth pressure coefficient was calculated by Coulomb theory using equation (4).

$$k_a = \frac{\cos(\varphi+\omega)^2}{\cos\omega^2\cos(\delta-\omega)\left[1+\sqrt{\frac{\sin(\varphi+\delta)\sin\varphi}{\cos(\delta-\omega)\cos\omega}}\right]^2} \tag{4}$$

where φ: friction angle; ω = facing inclination angle ; δ: soil-facing friction ratio

AASHTO (2012) conception method assumes that the location of peak tensile strength in each geogrid layer represents the internal failure surface. It should be noted that many of the experimental research and modeling work were consistent with the AASHTO (2012) design method (Djebablah (2020), Rahmouni (2016), Yang (2011), Rowe and Ho (1997) and Ho (1993)).

The orientation of the internal failure plane, α, can be calculated using the Coulomb's theory given by equation (5) for inclined reinforced retaining walls with (ω ≥ 10°). For reinforced soil retaining walls (ω < 10°), AASHTO (2012) ignores parameters: facing inclination angle and soil-facing friction ratio (δ = w = 0°), which equation (6) represents the Rankine's theory.

$$\tan(\alpha-\varphi) = \frac{-\tan\varphi + \sqrt{\tan\varphi[(\tan\varphi+\cot(\varphi+\omega))(1+\tan(\delta-\omega)\cot(\varphi+\omega)]}}{1+\tan(\delta-\omega)(\tan\varphi+\cot(\varphi+\omega))} \tag{5}$$

$$\alpha = \frac{\pi}{4} + \frac{\varphi}{2} \tag{6}$$

where: α: internal failure surface angle; ϕ: friction angle; ω: facing inclination angle; δ: soil-facing friction ratio.

Figure 13 illustrates the effect of facing inclination angle (ω) on the failure surface determined by the position of the peak tensile strength across the toe of the facing.

For facing inclination angles greater than 10° from the vertical, the present study was in good agreement with the results by Rahmouni (2016), Yang (2011), and Woodruff, R. (2003), where the internal failure is parabolic. In addition, the failure surface was greater than that predicted by the Rankine failure plane, and it is close to that defined by Coulomb.

For facing inclination angles smaller than 10°, the critical failure surface was quasi-linear. The peak tensile strength farthest from the wall was situated near Rankine's failure surface.

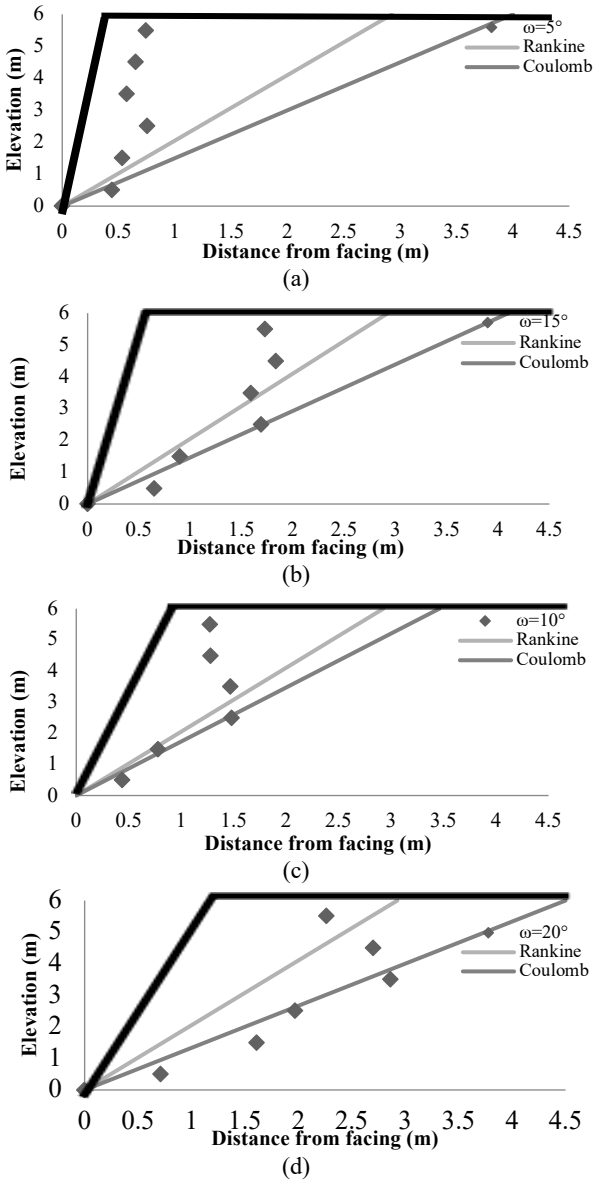

Figure 13 Location of internal failure surface with: (a) ω = 5°; (b) ω = 10°; (c) ω = 15°;(d) ω = 20°

3.7 Effect of Geogrid Inclination Angle (λ)

The general consideration when choosing the effect of geogrid inclination angle (λ) was to be able to achieve the internal stability of

the geogrid-reinforced soil retaining walls. Three different positions were examined as follows: λ = 0°, 5°, 10°.

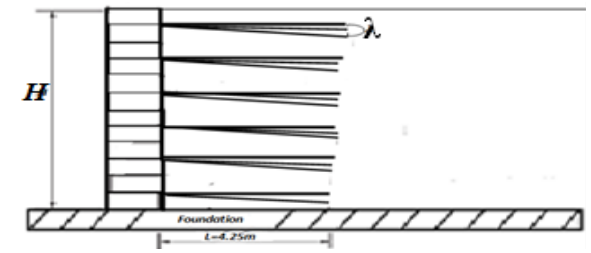

(a)

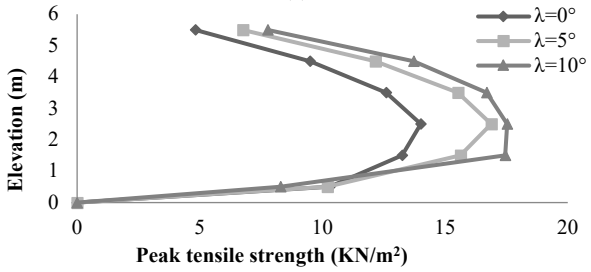

(b)

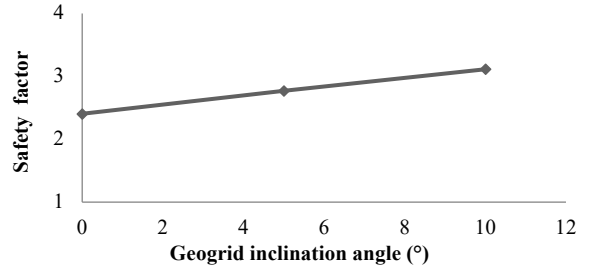

(c)

Figure 14 (a) Position of geogrid,(b) Effect of the geogrid inclination angle on peak tensile strength, (c) Safety factors

The variation of the geogrid inclination angle of the peak tensile strength is presented in Figure 14(b). According to the curves trend, it can be distinguished that the peak tensile strength increases with increasing geogrid inclination angle, and it was obtained at the mid-height of the reinforced zone. The peak tensile strength distribution becomes trapezoidal in shape. However, the influence of the geogrid inclination angle on the peak tensile strength was relatively small at the base of the reinforced retaining wall due to the foundation stiffness.

The safety factor value was given as a function of geogrid inclination angle, as illustrated in Figure 14(c). It can be seen that the safety factor increases with the inclination angle of the geogrid.

It can be inferred from Figure 15 that the lateral facing displacements decrease with increasing the geogrid inclination angle, and it concentrates on the third upper part of the wall about 2 m from the crest, and the geogrid-reinforced soil retaining wall fails internally. Considering the results, it could be concluded that the geogrid inclination angle has a major effect on the lateral facing displacements.

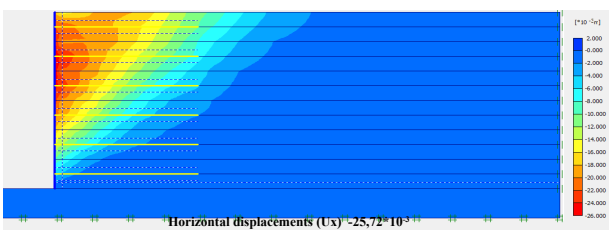

(a)

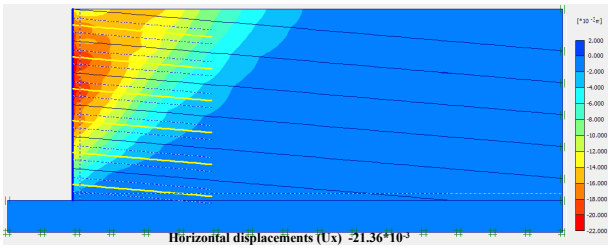

(b)

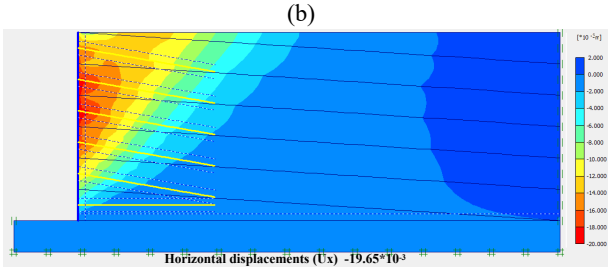

(c)

Figure 15 Effect of geogrid inclination angle on lateral facing displacement: (a) λ = 0°; (b) λ = 5°; (c) λ = 10°

3.8 Effect of Geogrid-Soil Friction Factor (δ_{rs})

To evaluate the effect of geogrid-soil friction factor (δ_{rs}) on the behavior of reinforced soil retaining wall with a segmental facing, some numerical analyses were carried out with different values: (δ_{rs} = 1/6φ, 1/3 φ, 4/7 φ, 2/3 φ, φ).

Corresponding to Figure 16, the geogrid-soil friction factor (δ_{rs}) does not appear to have any significant effect on the behavior of reinforced soil retaining wall for values δ_{rs} greater than 0.6ϕ. In this case, the critical value of δ_{rs} was in the order of 0.6 φ. It is important to notice that this conclusion seems to be in accordance with the results obtained by some authors, such as Rowe and Ho (1997), concerning the relationship between the reinforcement -soil friction factor and peak tensile strength is almost unique for values δrs greater than 2/3 φ. In addition, the friction factor required for calculating the minimum length of reinforcement layers recommended by AASHTO (2012) is equal to 0.67 tan φ.

For δ_{rs} less than 0.6 φ, the lateral facing displacement increases due to sliding between the geogrid and soil; this also means a reduction in the peak tensile strength in geogrid layers.

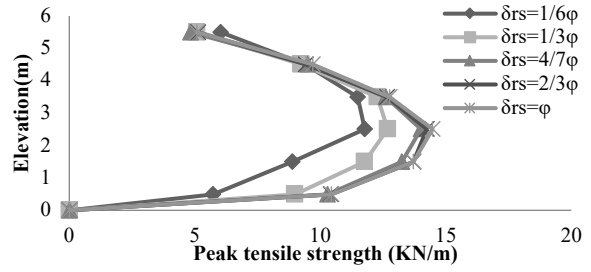

(a)

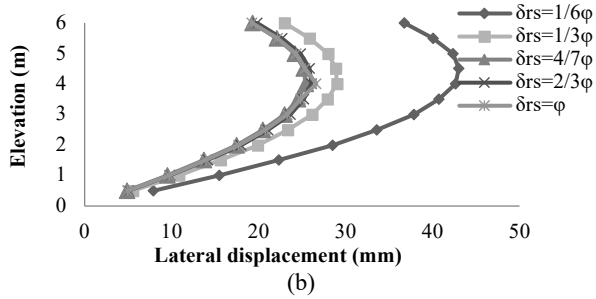

(b)

Figure 16 Effect of the geogrid-soil friction factor on (a) peak tensile strength, (b) lateral facing displacement

4. CONCLUSIONS

The objective of this study is to carry out modeling of the geogrid-reinforced soil retaining wall, using the finite element method with PLAXIS^{2D} code, in order to understand the behavior of this structure and to evaluate the influence of some geometrical and mechanical parameters, especially on the peak tensile strength in the geogrid layers, and on the lateral displacement of the wall. For the validation of our numerical model, the results obtained in this research are compared to those obtained by Djebablah et al. (2020), Vieira et al. (2008), and Rowe and Ho (1997). The following conclusions may be drawn:

- The facing panel type does not affect maximum tensile strength in geogrid layers and numerically defined lateral displacement of facing (continuous or segmented), which remains close.
- The mobilization of peak tensile strength increases proportionally with loading increments. Also, the distribution of peak tensile strength was quasi-linear at high-loading increments and trapezoidal at low-loading increments.
- The critical value of peak tensile strength was located at approximately the mid-height above the base of the wall. This examination does not follow the triangular distribution with depth assumed in geogrid-reinforced retaining wall conception methodologies.
- The peak tensile strength and the lateral facing displacement are not dependent on the loading increments width beyond 0.5H, which coincides with the Rankine's failure surface.
- The loading increments' location can change the shape and the position of the peak tensile strength, which is more pronounced for the higher loading values.
- The AASHTO (2012) conception method overestimating the length of reinforcement layer has been proposed as a function of the failure line geometry.
- The present study is in agreement with the AASHTO (2012) conception method, according to which the failure surface was based on the Rankine plane for a vertical facing and the Coulomb plane with an inclined facing ($\omega \geq 10°$).
- The geogrid inclination angle has a major effect on the lateral facing displacements and safety factor, the lateral displacements decrease with increasing geogrid inclination angle, and the critical mechanical failure model was generally the internal failure given by PLAXIS^{2D}.
- The soil-geogrid friction ratio is not considered to have a major effect on the peak tensile strength value for friction ratio greater than $4/7\phi$. In this case, the critical value of δ_{rs} is in the order of $0.6\ \phi$. However, the AASHTO (2012) method takes this parameter into account in the calculation of the minimum length of the resistant zone.

5. REFERENCES

AASHTO. (2012). "LRFD Bridge Design Specifications, Customary U. S. Unit 2012." *American Association of State Highway and Transportation Officials,* Washington, DC, U.S.A.

Bathurst, R. J. and Hatami, K. (1998). "Seismic Response Analysis of a Geosynthetic-Reinforced Soil Retaining Wall." *Geosynthetics International,* Vol. 5, Nos. 1–2, 127–166. DOI: 10.1680/gein.5.0117.

Haza, E. (1997). "Geosynthetic Reinforced Structures, Locally Loaded at the Head: Experimentation and Calculation Method." These.

Ho, See Keung. (1993). "A Numerical Investigation into The Behaviour of Reinforced Soil Walls." *Thesis,* Univ. of Western at Ontario, London. /ir.lib.uwo.ca/digitizedtheses/2298.

Mariano Linhares R, Mirmorad SH, and Ehrlich M. (2021). "Evaluation of the Effect of Surcharge on the Behavior of Geosynthetic-Reinforced Soil Walls." *Transportation Geotechnics Journal,* 31-100634, https://doi.org/10.1016/j.trgeo.2021.100634.

Mirmoradi SH and Ehrlich M. (2019). "Experimental Evaluation of the Effects of Surcharge Width and Location on Geosynthetic-Reinforced Soil Walls." *Int J Phys Model Geotechnics,* https://doi.org/ 10.1680/jphmg.16.00074.

Laboudi, K., Rahmouni, O., Labed, M. et al. (2022). "Numerical and Analytical Analysis of the Surcharge Application Distance Influence on the Behavior of Reinforced Soil Retaining Wall." *Indian Geotech J,* https://doi.org/10.1007/s40098-022-00680-6.

O. Rahmouni, A. Mabrouki, D. Benmeddour, and M. Mellas. (2016). "A Numerical Investigation into the Behavior of Geosynthetic-Reinforced Soil Segmental Retaining Walls." *International Journal of Geotechnical Engineering.*

Plaxis 2D (2004). "Plaxis Finite Element Code for Soil and Rock Analysis Manual." *Delft University of Technology and Plaxis, Delft,* The Netherlands.

Rowe, K. and Ho, K.S. (1997). "Continuous Panel Reinforced Soil Walls on Rigid Foundation." *Journal of Geotechnical and Geoenvironmental Engineering,* 10.1061/(ASCE) 1090 0241(1997)123:10(912), 912–920.

Vieira C. S., Lopes M. L., and Caldeira L. M. (2008). "Influence of Facing Panel Rigidity on Performance of Reinforced Soil Retaining Walls: A Numerical Study." *Proceedings of the 4th European Geosynthetics Conference,* Paper 244, Edinburg.

Wafa Djebablah, Mohamed Salah Nouaouria, and Souhila Adjabi. (2020). "Numerical Study of the Behaviour of Geosynthetic-Reinforced Soil Retaining Walls under a Uniform Surcharge." *International Journal of Structural Engineering.*

Woodruff, R. (2003). "Centrifuge Modeling of MSE-Shoring Composite Walls." *Thesis,* Univ. of Colorado, Boulder.

Yang, K. H., Utomo, P., and Liu, T. L. (2013). "Evaluation of Force-Equilibrium and Deformation Based Design Approaches for Predicting Reinforcement Loads within Geosynthetic Reinforced Soil Structures." *Journal of GeoEngineering,* 8, (2), 41–54.

Yang, K.H., J.G. Zornberg, C.N. Liu, and H.D. Lin (2012). "Stress Distribution and Development within Geosynthetic-Reinforced Soil Slopes." *Geosynthetics International,* 19(1): 62-78. DOI :10.1680/gein.2012.19.1.62.

Yang, K.H., Zornberg, J.G., Hung, W.Y., and Lawson, C.R. (2011). "Location of Failure Plane and Design Considerations for Narrow G.R.S. Wall Systems." *Journal of GeoEngineering,* Vol. 6, No. 1, April, 27-40.

Zornberg, J. G. and Arriaga, F. (2003). "Strain Distribution within Geosynthetic-Reinforced Slopes." *Journal of Geotechnical and Geoenvironmental Engineering,* ASCE, 131, No. 2, 141–150.